EBioMedicine 48 (2019) 554–567

Contents lists available at ScienceDirect

EBioMedicine

journal homepage: www.elsevier.com/locate/ebiom

EBioMedicine
Published by THE LANCET

Research paper

Accumulation of mitochondrial 7S DNA in idiopathic and LRRK2 associated Parkinson's disease

Petar Podlesniy[a,d,*], Margalida Puigròs[a,d], Núria Serra[a,d], Rubén Fernández-Santiago[b,c,d], Mario Ezquerra[b,c,d], Eduardo Tolosa[b,c,d], Ramon Trullas[a,c,d,**]

[a] Neurobiology Unit, Institut d'Investigacions Biomèdiques de Barcelona, Consejo Superior de Investigaciones Científicas (CSIC), Spain
[b] Neurology Service, Parkinson's Disease and Movement Disorders Unit, Institut Clínic de Neurociències, Hospital Clínic de Barcelona, University of Barcelona, Spain
[c] Institut d'Investigacions Biomèdiques August Pi i Sunyer (IDIBAPS), Spain
[d] Centro de Investigación Biomédica en Red Enfermedades Neurodegenerativas (CIBERNED), Barcelona, Spain

ARTICLE INFO

Article history:
Received 8 March 2019
Revised 3 September 2019
Accepted 6 September 2019
Available online 17 October 2019

Keywords:
mtDNA
Digital PCR
7S DNA
Parkinson's disease
LRRK2
G2019S LRRK2 missense mutation

ABSTRACT

Background: Both idiopathic and familial Parkinson's disease are associated with mitochondrial dysfunction. Mitochondria have their own mitochondrial DNA (mtDNA) and previous studies have reported that the release of mtDNA is a biomarker of Parkinson's disease.

Methods: We have now investigated the relationship between mtDNA replication, transcription and release in fibroblasts from patients with idiopathic (iPD) and Leucine-rich repeat kinase 2^{G2019S} -associated Parkinson's disease (LRRK2-PD), using Selfie-digital PCR, a method that allows absolute quantification of mtDNA genomes and transcripts.

Findings: In comparison with healthy controls, we found that fibroblasts from patients with iPD or LRRK2-PD had a high amount of mitochondrial 7S DNA along with a low mtDNA replication rate that was associated with a reduction of cf-mtDNA release. Accumulation of 7S DNA in iPD and LRRK2-PD fibroblasts was related with an increase in H-strand mtDNA transcription.

Interpretation: These results show that 7S DNA accumulation, low mtDNA replication, high H-strand transcription, and low mtDNA release compose a pattern of mtDNA dysfunction shared by both iPD and LRRK2-PD fibroblasts. Moreover, these results suggest that the deregulation of the genetic switch formed by 7SDNA that alternates between mtDNA replication and transcription is a fundamental pathophysiological mechanism in both idiopathic and monogenic Parkinson's disease.

* Correspondence to: P. Podlesniy, Neurobiology Unit, IIBB/CSIC, CIBERNED, c/Rosselló 161, sexta planta, Barcelona 08036, Spain.
** Correspondence to: R. Trullas, Neurobiology Unit, IIBB/CSIC, IDIBAPS, CIBERNED, c/Rosselló 161, sexta planta, Barcelona 08036, Spain.
E-mail addresses: petar.podlesniy@iibb.csic.es (P. Podlesniy), ramon.trullas@iibb.csic.es (R. Trullas).

https://doi.org/10.1016/j.ebiom.2019.09.015

Research in context

Evidence before this study

Accumulating evidence from several studies indicates that mitochondrial dysfunction is a pathophysiological mechanism in which different causes of Parkinson's disease converge. Further support for this hypothesis comes from reports showing that the majority of genes that cause familial Parkinson's disease alter mitochondrial function or dynamics. Mitochondria have their own mitochondrial DNA and recent studies have shown changes in the concentration of mitochondrial DNA in cerebrospinal fluid from patients with Parkinson's disease. However, whether these changes relate with altered mitochondrial DNA dynamics in Parkinson's disease is not well known.

Added value of this study

The study of mitochondrial DNA replication and transcription has been limited by the difficulty of accurately measuring the number of mitochondrial genome copies. To overcome this limitation, we developed a method called SelfiedPCR that allows absolute quantification of the number of mitochondrial RNA transcripts relative to their own transcription chain in the mitochondrial genome. Using this method, we found that primary fibroblasts obtained from patients with either idiopathic or LRRK2 Parkinson's disease share a similar dysfunction of the mitochondrial DNA replication and transcription machinery, including accumulation of 7S DNA, low mitochondrial DNA replication, high heavy strand transcription and low mitochondrial DNA release.

Implications of all the available evidence

The present results suggest that analysing mitochondrial DNA replication, transcription and release in fibroblasts may be an effective approach to investigate the biochemical pathways involved in Parkinson's disease and to identify new pharmacological targets. In addition, the available evidence supports the hypothesis that the gene switch that allows alternating mitochondrial DNA replication and transcription is a key mechanism in the pathophysiology of Parkinson's disease.

1. Introduction

Most cases of Parkinson's disease (PD) are diagnosed as idiopathic (iPD) because their aetiology is unknown. However, for between 5% and 10% of patients, the cause of PD is a genetic mutation. To date, a number of gene mutations have been identified that cause monogenic PD with autosomal inheritance [1]. Furthermore, several genetic variants increase the risk of developing iPD. However, albeit etiological diversity exists, both idiopathic and genetic PD show in most cases a similar clinical pattern of progressive neurodegeneration, suggesting that the molecular mechanisms in which the different gene mutations converge to induce the familial form of the disease are equivalent to those that underlie iPD.

Amongst the genes identified so far, mutations in the Leucine-rich repeat kinase 2 (LRRK2) gene represent the most common genetic cause of late-onset PD [2,3]. To date, six dominant mutations that cause PD have been found in the LRRK2 gene, but the most frequent is the missense variant G2019S [4], located in the kinase domain. Penetrance of LRRK2 mutations is incomplete and increases progressively with age [4,5], suggesting the involvement of yet unknown mechanisms that underlie the manifestation of the disease. The analysis of LRRK2 mutation carriers, together with that of patients with iPD provides a unique opportunity to identify fundamental pathophysiological mechanisms in which different causes converge to induce the disease. Thus, we have investigated replication, transcription, and release of mitochondrial DNA (mtDNA) in fibroblasts from both asymptomatic and PD manifesting LRRK2^{G2019S} mutation carriers and in fibroblasts from iPD and control patients. The use of fibroblasts is supported by previous reports showing that fibroblasts obtained from patients with familial or sporadic PD have impaired mitochondrial function, morphology and mitophagy [6–8], indicating that mitochondrial dysfunction is systemic in PD. In comparison with induced pluripotent stem cells, in which cellular reprogramming and clonal expansion change mtDNA dynamics [9], primary cultures of fibroblasts provide a more appropriate model to identify molecular mechanisms related with mitochondrial dysfunction.

A large body of evidence indicates that mitochondrial dysfunction is involved in the pathophysiology of PD (reviewed in [10,11]). Most of the genes that cause familial PD, including LRRK2, modify the mitochondrial function or dynamics [12]. Mitochondria have their own mtDNA that regulates mitochondrial function. There are multiple copies of mtDNA per cell and its number may vary by orders of magnitude depending on the cell type. The mitochondrial genome is tightly packed in nucleoids that are normally attached to the matrix side of the inner mitochondrial membrane. However, recent studies have identified circulating cell-free (cf) mtDNA in the cerebrospinal fluid and changes in its concentration are associated with PD [13–15], suggesting that mtDNA dynamics or expression are dysfunctional in PD patients.

The regulation of mtDNA dynamics involves different levels of control of mtDNA replication and transcription (reviewed in [16,17]). Mammalian mtDNA is a circular, double-stranded DNA molecule composed of a heavy (H) and light (L) strands, named by their buoyant sedimentation density. The mtDNA sequence has a noncoding region known as the mtDNA control region that contains transcription promoters for each strand as well as the origin of the H-strand replication. In a variable proportion of mammalian mtDNA molecules, the control region also contains a third strand of a variable length of around 650 bases known as 7S DNA, or D-DNA because it forms a displacement loop (D-loop) structure [18–20]. The presence of 7S DNA causes an open conformation in the mtDNA molecule that has been hypothesized to contribute to the regulation of mtDNA transcription [16,21,22]. Converging lines of evidence indicate that mtDNA replication and transcription are mutually exclusive processes [23,24], implying that 7S DNA is part of a regulatory switch that serves to avoid collision of replication and transcription machinery, which assemble within the mtDNA control region [23]. To test the hypothesis that alteration of this regulatory switch might underlie the dysfunction of mtDNA release previously observed in PD [13–15] we have investigated mtDNA replication and transcription in fibroblasts from patients with familial and idiopathic Parkinson's disease.

2. Materials and methods

2.1. Fibroblast primary culture

Primary cultures of fibroblasts were obtained from punch skin biopsies obtained from a total of 17 subjects classified in four different groups based on clinical diagnosis and genotype: 1) NMNC, non-manifesting non-carriers; subjects who do not carry the LRRK2 ^{G2019S} mutation and do not manifest PD at the time of enrolment, $n = 4$. 2) iPD, idiopathic PD; subjects with confirmed clinical diagnosis of idiopathic PD but that do not carry the LRRK2 ^{G2019S} mutation, $n = 4$. 3) NMC, non-manifesting carriers; subjects who carry the LRRK2 ^{G2019S} mutation and do not manifest

Table 1
Patient characteristics.

Group	*n*	Age at biopsy (years)	Gender M/F	LRRK2-Mutation
NMNC	4	59 ± 5	2/2	None
iPD	4	57 ± 4	2/2	None
NMC	5	50 ± 3	2/3	G2019S
LRRK2-PD	4	57 ± 5	2/2	G2019S

Fibroblast lines were obtained from 17 subjects from the Parkinson's disease and Movement Disorders Unit of the Hospital Clínic de Barcelona. NMNC (non-manifesting non-carriers): subjects who do not carry a mutation in the LRRK2 gene that do not manifest Parkinson's disease at the time of enrollment. iPD: subjects who do not carry a mutation in the LRRK2 gene but have a confirmed diagnosis of idiopathic Parkinson's disease. NMC (non-manifesting carriers): subjects who carry the G2019S mutation in the LRRK2 gene but do not manifest Parkinson's disease. LRRK2-PD: subjects who carry the G2019S mutation in the LRRK2 gene and have Parkinson's disease. *n* = number of subjects. Values are mean ± SEM.

PD, $n = 5$. 4) LRRK2-PD, subjects with the LRRK2 ^{G2019S} mutation who manifest clinical signs of PD, $n = 4$. All participants were assessed for clinical characteristics based on the Movement Disorder Society-sponsored revision of the Unified Parkinson's disease Rating Scale (MDS-UPDRS) [25]. The characteristics of patient groups are described in Table 1. The ethics committee from the Hospital Clínic of Barcelona approved the study (statement 2011/6704). All patients signed an informed consent declaration before the collection of the fibroblasts sample. A line of fibroblasts from each subject from the four different groups was established. There was no significant difference in age between the control and patient groups.

Primary fibroblasts were cultured in Dubecco's modified Eagle medium (Ref. 31966-047, ThermoFisher, RRID:SCR_008452) with 10% fetal bovine serum (Ref. 10500-064, ThermoFisher, RRID:SCR_008452) and 0.2% gentamicin (Ref. 15750-037, ThermoFisher, RRID:SCR_008452). To ensure that fibroblasts from each group were studied in the same conditions and at the same passage, fibroblasts from each patient were expanded up to passage #5 and stored in liquid nitrogen in aliquots of 0.5×10^6 cells. For each experiment, aliquots of passage #5 were quickly defrost at 37 °C, plated in a 70 cm^2 dish with fresh medium, incubated at 37 °C and the medium replaced 24 h after plating. Three days later, cells were trypsinized (Ref. 15090046, ThermoFisher, RRID:SCR_008452), counted with trypan blue (Ref. 1450022, Bio-Rad Laboratories, RRID:SCR_008426) and plated at 7000 cells/cm2 in 6-well dishes (Ref. 30720113, Eppendorf, RRID:SCR_000786) previously coated with poly-D-Lysine (Ref. P0899-50MG, Sigma-Aldrich, RRID:SCR_008988). After 2 h of incubation at 37 °C to allow the cells to attach to the culture plate, the medium was replaced with fresh medium and fibroblasts were lysed four hours later. In some experiments, fibroblasts were treated with serum deprivation during the last 4-h period. The total 6-h period was adopted because characterization studies indicated there were no significant differences in cell number due to different cell proliferation rates between the fibroblast lines after this time in culture. All studies were performed at passage #7 for all fibroblast groups.

2.2. Sample preparation

To preserve the native ratio between nuclear and mitochondrial nucleic acids, Selfie-digital PCR analysis was performed using sample lysate without nucleic acid extraction as previously described [26]. Briefly, media was aspirated from culture wells and fibroblasts were lysed in 100ST DNA/RNA/Protein Solubilization Reagent (#DCQ100ST, DireCtQuant) at 250 cells/ul. The lysate was incubated at 90 °C for 3 min with 750 rpm agitation, centrifuged at 10.000 rcf for 10 min and used directly to measure mtDNA, 7SDNA, nuclear DNA and mtRNA.

2.3. Determination of mtDNA copy number

Measurement of the absolute copy number of mtDNA per diploid genome was performed by droplet digital PCR (dPCR) with two different primer pairs, mt64-ND1 and mt92-CYTB. These primer pairs target two opposite regions of the mtDNA genome that are outside the majority (>90%) of the mtDNA deletions reported [27,28] (primer sequences and amplicon characteristics are described in Table 2). The number of diploid genomes was measured by multiplex amplification of two single copy nuclear genes: human TATA-box binding protein 1 (TBP73 amplicon) and mitochondrial transcription elongation factor (TEFM88 amplicon). Measurement of two single copy genes simultaneously in a multiplex ddPCR reaction significantly improves precision by reducing sampling error. Analyses were performed using amplitude multiplex with EvaGreen in a QX200 Digital Droplet PCR platform (Bio-Rad Laboratories, RRID:SCR_008426). The digital droplet reaction consisted of 1× QX200™ ddPCR™ EvaGreen Supermix (1864033, Bio-Rad, RRID:SCR_008426), an aliquot of target sample (1ul for diploid genome determination and 0,001ul for mtDNA measurement) and DNA primers at the concentration specified in Table 2. A restriction enzyme digestion was performed for 15 min at 37 °C before partition in droplets by addition into the ddPCR reaction of 1 U of the Fast Digest enzyme required for the corresponding amplicon as described in Table 2. Non-template controls were included in each analysis plate to monitor possible reaction contamination. Data analysis was performed with QuantaSoft Analysis Pro v1.0 using thresholds to distinguish single and double positive droplet populations. The number of diploid genomes was calculated by dividing by four the sum of TBP73 and TEFM88 genome copies. To determine the amount of mtDNA copies per diploid genomes, the number of mtDNA copies obtained with the mt64-ND1 or the mt92-CYTB amplicon was divided by the number of diploid genomes measured in the same sample. The specificity of the primers was assessed by BLAST analysis versus the human reference genome database and all the primer pairs used in our studies were found to be unique to the intended targets. Amplification specificity and absence of non-specific amplification was also verified by analysing amplicon size by agarose gel electrophoresis. To rule out the possibility that the primer pairs mt64-ND1, mt92-CYTB and mt86-7S amplify non-specific targets in nuclear DNA, we measured mtDNA copy number in the rho-zero human osteosarcoma cell line 143B rho-0#25 (RRID:CVCL_XF76), a cell line depleted of mtDNA commonly used as recipient in the production of cytoplasmic hybrids, and the respective control cell line (Supplementary Fig. 1). The PCR amplification was performed using the following thermal profile: 95 °C 5 min; (95 °C 30s; 60 °C 1 min) 40 repeats; 4 °C 5 min; 90 °C 10 min using the C1000 Touch Thermal Cycler (Bio-Rad).

2.4. Measurement of 7S DNA

Some mtDNA molecules contain a third strand of a variable length of around 650 bases bound to the H-strand in the control region known as 7S DNA (Fig. 1a). We measured the amount of mtDNA molecules containing 7S DNA by means of digital PCR, which allows quantification of distinct mtDNA regions when separated in different partitions. To determine specifically the number of mtDNA molecules that contain 7S DNA we developed a multiplex digital PCR assay using two different primer combinations, mt92-CYTB and mt86-7S. The mt92-CYTB primer combination amplifies the region between bases 15427 and 15518 of the mtDNA sequence that is outside the control region and measures the total number of mtDNA molecules. On the other hand, the mt86-7S primer combination targets a control region that contains 7S DNA and the four base pair restriction endonuclease *Alu*I site just before and after the mt86-7S amplicon. In the absence of 7S

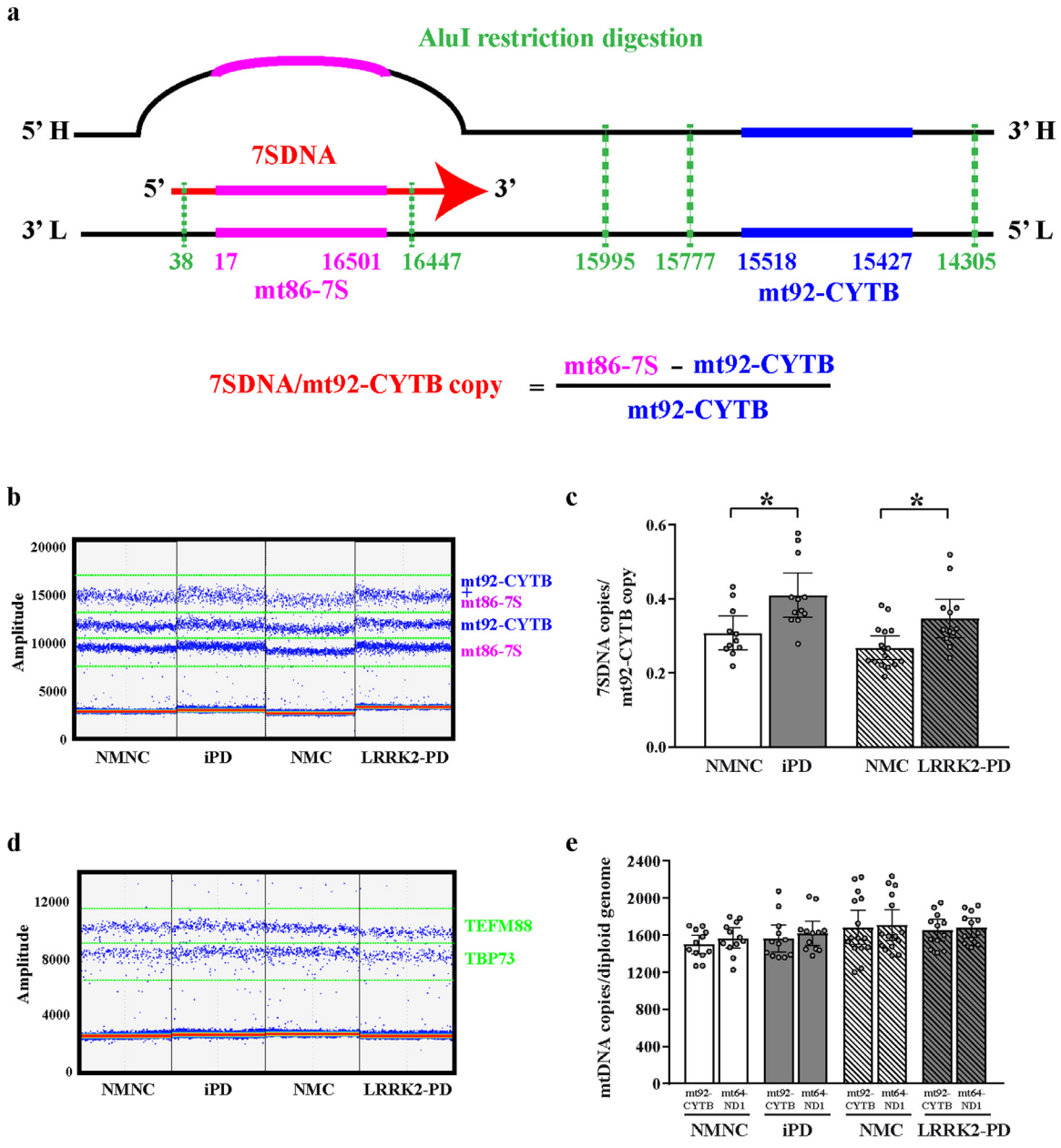

Fig. 1. Increased mitochondrial 7S DNA in iPD and LRRK2-PD. a) Schematic diagram of mtDNA regions amplified by the two primer pairs used to measure the number of mtDNA molecules that contain 7S DNA in a multiplex digital PCR assay. The mt92-CYTB primer pair (thick blue lines) amplifies the region outside the D-loop between bases 15,427 and 15,518 of the mtDNA sequence, measuring total mtDNA copy number. The mt86-7S primer pair (thick pink lines) amplifies the region between bases 16,501 and 17 of the D-Loop, measuring the mtDNA copy number plus the number of 7S DNA fragments (red arrow). Subtracting mt92-CYTB amplicons from mt86-7S amplicons and dividing the result by the number of mt92-CYTB amplicons yields the amount of 7S DNA copies per mtDNA copy. Dotted green lines represent *Alu*I restriction sites within this region. b) Representative one dimension (1-D) droplet scatter plot of mt92-CYTB and mt86-7S amplicons after droplet digital PCR. Blue dots above an amplitude of 5000 indicate droplets positive for mt86-7S, mt92-CYTB or mt86-7S + mt92-CYTB amplicons. NMNC (non-manifesting non-carriers): control subjects who do not carry a mutation in the LRRK2 gene and do not manifest Parkinson's disease at the time of enrollment. iPD, subjects who have a confirmed clinical diagnosis of idiopathic Parkinson's disease but do not carry a LRRK2 mutation. NMC (non-manifesting carriers), subjects who carry the G2019S mutation in the LRRK2 gene and do not manifest Parkinson's disease. LRRK2-PD, subjects who carry the G2019S mutation in the LRRK2 gene and have Parkinson's disease. c) Quantification of 7S DNA copies/mtDNA copy in fibroblast samples from each group by dPCR. Data are mean and 95% CI. NMNC, $n = 11$, 4 lines; iPD, $n = 12$, 4 lines; NMC, $n = 15$, 5 lines, LRRK2-PD, $n = 12$, 4 lines. *, significantly different from the respective control group, $p < 0{\cdot}05$ (ANOVA with Fisher's LSD test). d) Representative 1-D droplet scatter plot of the number of diploid genomes measured by multiplex digital PCR amplification of two single copy nuclear genes: human TATA-box binding protein 1 (TBP73 amplicon) and mitochondrial transcription elongation factor (TEFM88 amplicon). e) Quantification of mtDNA copy number in fibroblasts from each group calculated using the amount of mt92-CYTB or mt64-ND1 amplicons in each sample divided by the amount of diploid genomes present in the same sample. Values are mean and 95% CI. NMNC, $n = 12$, 4 lines; iPD, $n = 12$, 4 lines; NMC, $n = 15$, 5 lines, LRRK2-PD, $n = 12$, 4 lines. *n* denotes number of independent experiments. (For interpretation of the references to colour in this figure legend, the reader is referred to the web version of this article.)

Table 2
Primer sequences.

mtDNA

Amplicon	5′-3′ sequence L-strand	5′-3′ sequence H-strand	Start position	End position	Sequence reference	Restriction enzyme	[Final] in ddPCR
mt92-CYTB	AGACGCCCTCGGCTTACTTC	GGGTATAATTGTCTGGGTCGCC	15,427	15,518	NC_012920.1	AluI	135 nM
mt86-7S	CTGGTTCCTACTTCAGGGTCATA	GTGATAGACCTGTGATCCATCGT	16,501	17	NC_012920.1	AluI	80 nM
mt64-ND1	ACTACAACCCTTCGCTGACG	AGATGTGGCGGGTTTTAGGG	3441	3504	NC_012920.1	AluI	100 nM
mt82-CYTB	ACAATTCTCCGATCCCGTCCC	TGGGGATTATTGCTAGGATGACG	15,581	15,662	NC_012920.1	AluI	100 nM
mt88-ND4	CAGCCACATAGCCCTCGTAG	CCCGTGGGCGATTATGAGAA	11,632	11,719	NC_012920.1	*Hae*III	100 nM

Nuclear DNA

Amplicon	5′-3′ sequence	5′-3′ sequence	Start position	End position	Sequence reference	Restriction enzyme	[Final] in ddPCR
TEFM88	GTGACTCCCGGACTAGTCGA	GATCGGAAGAACACCCGAGG	30,899,296	30,899,383	NC_000017.11, Chromosome 17, GRCh38.p7	HaeIII and *Mse*I	140 nM
TBP73	CACCACAGCTCTTCCACTCA	GGGGACGGATACAGTGGAGT	170,562,089	170,562,161	NC_000006.12, Chromosome 6, GRCh38.p7	HaeIII and MseI	95 nM

Primer sequences used in the present studies indicating start and end of the amplified region according to the base numbering of the corresponding reference sequence. The restriction enzyme and the final concentration of primer used in the dPCR reaction are also indicated.

DNA, the cleavage of mtDNA molecule by AluI results in a single mt86-7S amplicon from H- and L- strands. The presence of 7S DNA creates an additional AluI restriction site, which produces two mt86-7S amplicons that separate in different partitions containing the H-strand/7SDNA hybrid or the L-strand. The amount of mt86-7S amplicons represents the sum of mtDNA copies and 7S DNA fragments. Subtracting the number of mt92-CYTB amplicons from mt86-7S amplicons and dividing the result by the number of mt92-CYTB amplicons yields the amount of 7S DNA copies per mtDNA copy. We performed digestion with AluI enzyme in the digital PCR mix before the partitioning step. A schematic representation of the procedure is in Fig. 1a.

2.5. Cell-free mtDNA

Cf-mtDNA was measured in the cell culture medium after centrifugation at 10.000 *g* for 10 min to remove cells and cell debris. The number of copies of cell-free mtDNA was measured directly in 4.5 ul of culture medium by droplet digital PCR with two different primer pairs: mt92-CYTB and mt82-CYTB in the same PCR reaction as previously described [29].

2.6. Strand-specific mtDNA transcription quantification by Selfie-dPCR

Strand-specific analysis of mtDNA transcription was performed by Selfie-dPCR as previously described [26]. This method enables separate analysis of transcriptional activity of each one of the mtDNA strands without using a reference gene, a necessary requirement when the number of genomes is variable such in the case of mtDNA. We measured the absolute number of H- and L-mtDNA strand transcripts and expressed the results in two different forms: as transcripts/mtDNA copy and transcripts/diploid genome, to control for changes in mtDNA copy number and in cell number respectively (Fig. 3b-e). In addition, to control for the accuracy of quantification of H- and L- transcripts, we used two different primer combinations targeting two separate regions (Fig. 3a). The mt64-ND1 primer combination targets a region near the beginning of the H-strand transcript and at the end of the L-strand transcript (between bases 3441 and 3504), whereas the mt92-CYTB primer combination targets a region near the beginning of the L-strand transcript and at the end of H-strand transcript (between bases 15,427–15,518) (Fig. 3a). The Selfie-dPCR procedure includes four steps: 1) sample and mtRNA strand-specific primer pre-annealing in duplicate aliquots of the same sample, 2) reverse transcription with retro-transcriptase enzyme in one duplicate and no enzyme in the other duplicate, 3) restriction enzyme digestion after addition of the second primer pair, followed by digital PCR and 4) nucleic acid quantification. To prime the retro-transcription of the H-strand mtRNA we used the primer with the H-strand sequence and to prime the retro-transcription of the L-strand mtRNA we used the primer with the L-strand sequence (Table 2). To anneal the primers to their complementary transcripts, a reaction mixture containing the sample and 500 nM primer in 10ul of double distilled water was heated to 70 °C for 1 min, followed by a gradual decrease of temperature to 22 °C. Afterwards, we added 4 μl of reaction buffer 5× (EP0751, ThermoFisher, RRID:SCR_008452), 2 μl 10 mM dNTPs (R0191, ThermoFisher, RRID:SCR_008452), 0.5 μl Ribolock RNase inhibitor (EO0381, ThermoFisher, RRID:SCR_008452) and double-distilled water to a final volume of 19.5 μl to each duplicate. After mixing both tubes well, we added 0.5 μl of Maxima H Minus reverse transcriptase (EP0751, ThermoFisher, RRID:SCR_008452) to one of the duplicates and 0.5 ul of enzyme storage buffer to the second duplicate. Then, both tubes were incubated at 60 °C for 30 min to perform the retro-transcription, followed by 90 °C incubation for 3 min, to inactivate the reverse transcriptase. Next, 4 ul

of each duplicate were added to a ddPCR reaction mixture containing 100 nM of the corresponding primer, 1 U of *Alu*I restrictase (#FD0014, ThermoFisher, RRID:SCR_008452) and 1 x EvaGreen ddPCR Supermix in a final volume of 20 ul. After restriction digestion (15 min, 37 °C), the reaction was partitioned in 70 μl of droplet generation oil for EvaGreen (186-4005, Bio-Rad, RRID:SCR_008426) in a QX200 Droplet Generator. The emulsion was transferred to a 96-well plate. PCR was performed in a thermal cycler (C1000 Touch Thermal Cycler, Bio-Rad, RRID:SCR_008426) using the following thermal profile: 95 °C 5 min; (95 °C 30s; 60 °C 1 min) 40 repeats; 4 °C 5 min; 90 °C 10 min. Non-template controls containing all the reagents and the corresponding amount of solubilization buffer without sample lysate were included in all steps of the procedure. The number of mtRNA transcripts was calculated by subtracting the amount of amplicons measured in the reaction without reverse transcriptase (RT-) from the reaction with reverse transcriptase (RT+) and dividing by (RT-). The results were expressed in two different forms: as transcripts/mtDNA copy and transcripts/diploid genome, to control for changes in mtDNA copy number and in cell number respectively.

2.7. EdU incorporation and quantification

Fibroblast aliquots stored at passage #5 were quickly defrost at 37 °C and plated in 2 cm^2 wells (Ref. 0030722116, Eppendorf, RRID:SCR_000786) containing 12 mm #1.5 coverslips (Ref. 11846933, ThermoFisher, RRID:SCR_008452) previously coated with poly-D-lysine. Fibroblasts were cultured up to passage #7 as described in the primary culture section. In the last passage, fibroblasts were incubated with medium containing 20 uM of 5-Ethynyl-2′-deoxyuridine (EdU) for 4 h, fixed and permeabilized using the Click-iT Plus EdU Alexa Fluor 647 Imaging Kit (Ref. C10640, ThermoFisher, RRID:SCR_008452). Cell nucleus was stained with Picogreen (Ref. P11495, ThermoFisher, RRID:SCR_008452) at a dilution 1:1000. Coverslips were mounted with ProLong gold antifade (Ref. P36934, ThermoFisher, RRID:SCR_008452). Imaging was performed with a confocal microscope Leica TCS SPE (Leica Microsystems, RRID:SCR_002140) with a 63×/1.4 NA oil-immersion objective. Seven to ten cell images, chosen at random, were acquired per patient fibroblast line. A similar number of cells was analysed for each line in all groups. The quantification of EdU positive puncta was performed with FIJI Image J 1.47v (RRID:SCR_002285) [30] using the 3D Object Counter plugin (RRID:SCR_017066) [31] with a pixel intensity threshold of 15 (8-bit grayscale) and an object size filter of 10-500 voxels, corresponding to an object diameter between 147 and 540 nm. The number of puncta was measured in a blinded fashion using an Image J macro plugin that automatically quantified cell area, the number of EdU puncta per cell and EdU puncta volume using the 3D objects counter program.

2.8. Statistical analysis

Results are expressed as mean ± standard deviation (SD) in the text and as scatter dot plots with the mean and the 95% confidence interval (CI) in graphs. dPCR assays included samples from all groups in a balanced manner. No values were excluded for statistical purposes. Statistical analyses were performed with GraphPad Prism software v7 (RRID:SCR_000306) using one-way analysis of variance (ANOVA) with Fisher's least significant difference (LSD) post hoc tests or with two-tailed unpaired Student's *t*-tests where indicated. Differences were considered statistically significant at a value of $p < 0.05$. Cohen's d effect size was calculated for each significant difference between groups.

3. Results

3.1. 7S DNA and mtDNA copy number

In a first approach to study mtDNA dynamics, we measured 7S DNA, the D-loop DNA fragment bound to the L-strand in the mtDNA control region. To determine the number of mtDNA molecules containing 7S DNA we developed a novel multiplex digital PCR assay using two different primer combinations, mt92-CYTB and mt86-7S. The mt92-CYTB primer combination amplifies the region between bases 15427 and 15518 of the mtDNA sequence that is located outside the D-loop and measures the total number of mtDNA molecules. On the other hand, the mt86-7S primer combination amplifies the region between the bases 16501 and 17 of the D-Loop and measures the total number of mtDNA copies plus the number of 7S DNA fragments. Subtracting the number of mt92-CYTB amplicons from mt86-7S amplicons and dividing the result by the number of mt92-CYTB amplicons yields the amount of 7S DNA copies per mtDNA copy (Fig. 1a). Using this method, we found that fibroblasts from patients with iPD had a significant increase in the proportion of mtDNA molecules containing 7S DNA compared with healthy non-manifesting non-mutation carrier control subjects (NMNC). iPD $=0{\cdot}410 \pm 0{\cdot}093$ 7S DNA copies/mtDNA copy, $n = 12$, 4 fibroblast lines; NMNC $= 0{\cdot}308 \pm 0{\cdot}067$ 7S DNA copies/mtDNA copy, $n = 11$, 4 fibroblast lines (effect size d = 1·3). Likewise, fibroblasts from patients with LRRK2-PD showed a significant increase in the proportion of mtDNA molecules with 7S DNA compared with the corresponding non-manifesting carrier (NMC) control subjects. LRRK2-PD $=0{\cdot}348 \pm 0{\cdot}082$ 7 SDNA copies/mtDNA copy, $n = 12$, 4 fibroblast lines, NMC $= 0{\cdot}268 \pm 0{\cdot}058$ 7 SDNA copies/mtDNA copy, $n = 15$, 5 fibroblast lines (effect size d = 1·1) (Fig. 1b & c).

To obtain an absolute value of mtDNA copy number in the different fibroblast lines, we measured the number of diploid genomes in each sample to assess the precise amount of cells analysed. We measured simultaneously two different genes, TBP and TEFM, which we previously confirmed are single copy genes in the different fibroblast cell lines studied. We found that the number of mtDNA copies/diploid genome was not significantly different in iPD or LRRK2-PD fibroblasts from their respective controls, measured with either mt92-CYTB or mt64-ND1 amplicons (Fig. 1d & e). Overall, these results indicated that fibroblasts from both iPD and LRRK2-PD patients had more mtDNA molecules containing 7S DNA.

3.2. mtDNA replication

To determine whether the increase in 7S DNA found in fibroblasts from PD patients was associated with changes in mtDNA synthesis, we monitored the incorporation of 5-ethynyl-2′-deoxyuridine (EdU), a synthetic thymidine nucleotide analog that is incorporated into newly synthesized DNA and can be visualized in fixed cells using copper click chemistry [32]. Confocal microscopy images of fibroblasts obtained after incubation with 20 uM EdU for 4 h showed a high density of EdU labelled DNA in the cell nucleus and a number of EdU labelled puncta in the cytoplasm (Fig. 2a). Quantitative analysis of the images showed a significant decrease in the number of EdU puncta per cell in fibroblasts from patients with either iPD or LRRK2-PD, compared with their corresponding NMNC and NMC controls. iPD $= 66 \pm 32$, $n = 41$ fibroblasts, 4 lines, NMNC $= 89 \pm 39$, $n = 29$ fibroblasts, 4 lines (effect size d = 0·7). LRRK2-PD $= 67 \pm 22$, $n = 25$ fibroblasts, 3 lines, NMC $= 84 \pm 37$, $n = 36$ fibroblasts, 5 lines (effect size d = 0·6) (Fig. 2b).

To measure the proportion of mtDNA molecules that incorporated EdU during the 4 h incubation period, for each one of the

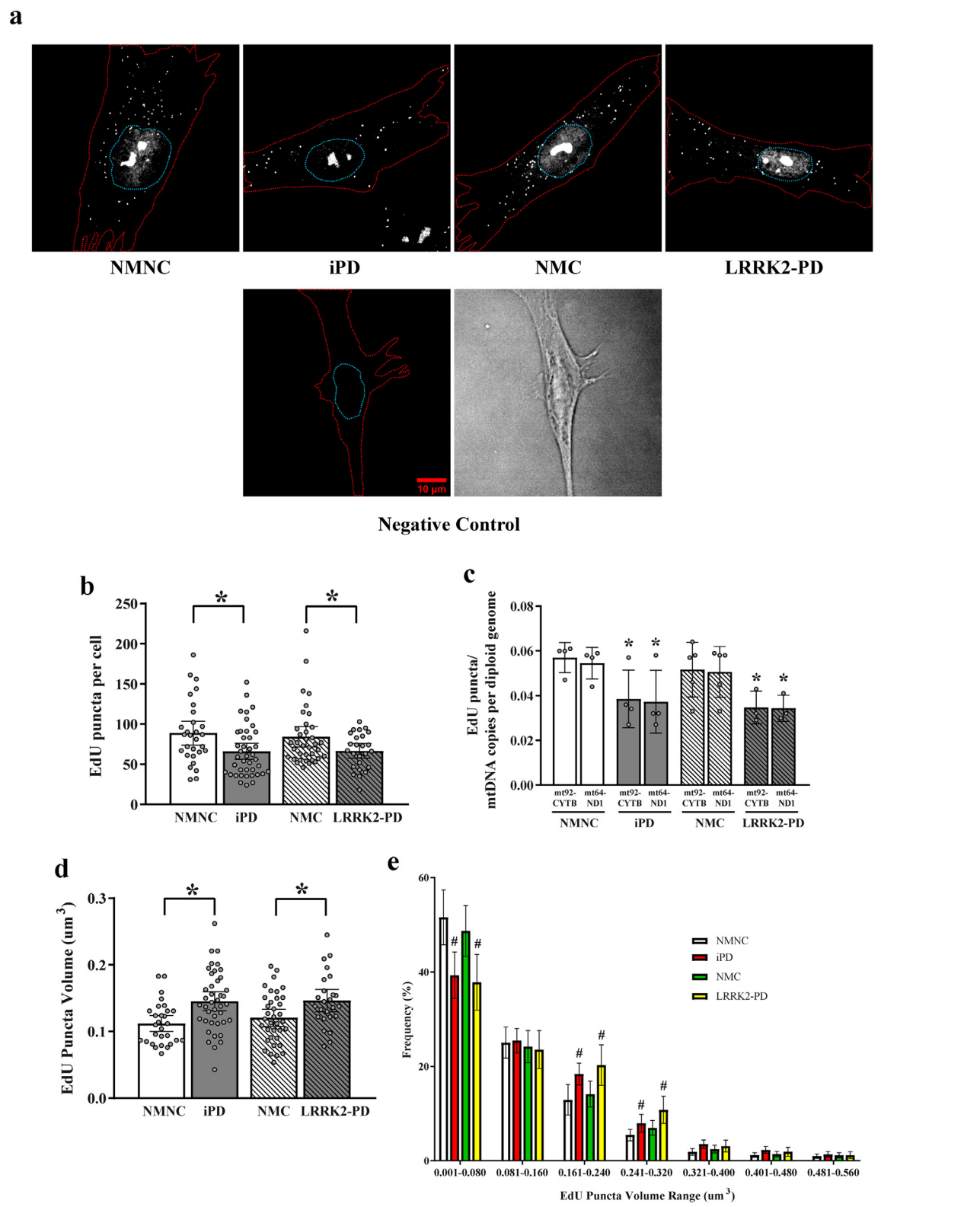

Fig. 2. Reduced mtDNA replication in iPD and LRRK2-PD. Replication was evaluated by incorporation of 5-ethynyl-2′-deoxyuridine (EdU) into newly synthesized mtDNA and confocal fluorescence imaging after labeling EdU with AlexaFluor 647. a) Representative maximal projection fluorescence images obtained with confocal microscopy of fibroblasts (delineated by a dotted red line) from each group after a 4 h pulse treatment with 20 uM EdU. Images show EdU mtDNA puncta (in white) in the cytoplasm and EdU labelled DNA in the cell nucleus (delineated by a dotted blue line). Only puncta between 200 and 618 nm diameter were considered for 3D particle analysis in ImageJ. Negative controls (shown are representative images of fluorescence, left panel, and differential interference contrast, right panel, of a control fibroblast) were subjected to the same procedure, but without addition of EdU. Scale Bar = 10 um. b) Quantification of EdU labelled mtDNA puncta per cell. NMNC, $n = 29$ fibroblasts, 4 lines; iPD $n = 41$ fibroblasts, 4 lines; NMC, $n = 36$ fibroblasts, 5 lines; LRRK2-PD, $n = 25$ fibroblasts, 3 lines. c) Quantification of EdU puncta calculated with mt92-CYTB or mt64-ND1 amplicon copies per diploid genome. NMNC, $n = 4$ lines; iPD $n = 4$ lines; NMC, $n = 5$ lines; LRRK2-PD, $n = 3$ lines. d & e) Volume of EdU labelled mtDNA puncta and frequency histogram. NMNC, $n = 29$ fibroblasts, 4 lines; iPD $n = 41$ fibroblasts, 4 lines; NMC, $n = 36$ fibroblasts, 5 lines; LRRK2-PD, $n = 25$ fibroblasts, 3 lines. All data are mean and 95% CI. *, significantly different from the respective control group, $p < 0{\cdot}05$ (ANOVA with Fisher's LSD test). #, significantly different from the respective control group, $p < 0{\cdot}05$, unpaired *t*-test. (For interpretation of the references to colour in this figure legend, the reader is referred to the web version of this article.)

fibroblast lines we calculated the ratio between the average number of EdU puncta per cell and mtDNA copy number per diploid genome measured with two different primer pairs, mt92-CYTB and mt64-ND1. The results showed that control groups do not differ in the proportion of newly synthesized mtDNA, which is on average approximately 5%, independently of the primer pair used to measure mtDNA copies per diploid genome (Fig. 2c). For mt92-CYTB: NMNC = 0·057 ± 0·007 EdU puncta/mtDNA copy, $n = 4$ lines and NMC = 0·052 ± 0·012 EdU puncta/mtDNA copy, $n = 5$ lines. For mt64-ND1: NMNC = 0·055 ± 0·007 EdU puncta/mtDNA copy, $n = 4$ lines and NMC = 0·051 ± 0·011 EdU puncta/mtDNA copy, $n = 5$ lines. In fibroblasts from LRRK2-PD patients, when compared to NMC controls, the synthesis of mtDNA was significantly reduced to 3·5% and 3·4% (effect size d = 1·7 and d = 1·9) for mt92-CYTB and mt64-ND1, respectively (Fig. 2c). For mt92-CYTB, 0·035 ± 0·007 EdU puncta/mtDNA copy, $n = 3$ lines. For mt64-ND1, 0·034 ± 0·006 EdU puncta/mtDNA copy, $n = 3$ lines. Likewise, in fibroblast lines from iPD patients, when compared to NMNC controls, the synthesis of mtDNA was significantly reduced to 3·9% and 3·7% (effect size d = 1·7 and d = 1·6) for mt92-CYTB and mt64-ND1 respectively (Fig. 2c). For mt92-CYTB, 0·039 ± 0·013 EdU puncta/mtDNA copy, $n = 4$ lines. For mt64-ND1, 0·037 ± 0·014 EdU puncta/mtDNA copy, $n = 4$ lines.

Morphological analyses revealed that the volume of EdU labelled mtDNA puncta was significantly larger in fibroblasts from iPD and LRRK2-PD patients (30% and 22%, effect size d = 0·85 and d = 0·66, vs fibroblasts from NMNC and NMC control subjects, respectively). iPD = 0·145 ± 0·045 um^3, $n = 41$ fibroblasts, $n = 4$ lines; LRRK2-PD = 0·146 ± 0·041 um^3, $n = 25$ fibroblasts, $n = 3$ lines, compared to NMNC = 0·112 ± 0·032, $n = 29$ fibroblasts, $n = 4$ lines and NMC = 0·120 ± 0·038, $n = 36$ fibroblasts in $n = 5$ lines, respectively (Fig. 2d). Subsequent analyses of the volume of EdU puncta showed that fibroblasts from iPD and LRRK2-PD patients exhibit a significant decrease in the number of small EdU puncta in the volume range within 0·001 and 0·080 um^3 (effect size d = 0·8 and d = 0·7 for iPD and LRRK2-PD, respectively). iPD = 39 ± 16 puncta, $n = 41$ fibroblasts, $n = 4$ lines; LRRK2-PD = 38 ± 14 puncta, $n = 25$ fibroblasts, $n = 3$ lines, compared to NMNC = 52 ± 15 puncta, $n = 29$ fibroblasts, $n = 4$ lines and NMC = 49 ± 16, $n = 36$ fibroblasts, $n = 5$ lines, respectively (Fig. 2e). This decrease in number of small EdU puncta in fibroblasts from iPD and LRRK2-PD patients corresponded with an increase in the number of large EdU puncta in volume ranges from 0·161 to 0·320 um^3. For the 0·161–0·240 um^3 range: iPD = 18 ± 7 puncta, $n = 41$ fibroblasts, $n = 4$ lines; LRRK2-PD = 20 ± 10 puncta, $n = 25$ fibroblasts, $n = 3$ lines, compared to NMNC = 13 ± 9 puncta, $n = 29$ fibroblasts, $n = 4$ lines and NMC = 14 ± 8, $n = 36$ fibroblasts, $n = 5$ lines (effect size d = −0·6 and d = 0·7, for iPD and LRRK2-PD, respectively). For the 0·241–0·320 um^3 range: iPD = 8 ± 6 puncta, $n = 41$ fibroblasts, $n = 4$ lines; LRRK2-PD = 11 ± 7 puncta, $n = 25$ fibroblasts, $n = 3$ lines, compared to NMNC = 5 ± 3 puncta, $n = 29$ fibroblasts, $n = 4$ lines, and NMC = 7 ± 5, $n = 36$ fibroblasts, $n = 5$ lines (effect size d = 0·6 and d = 0·7, for iPD and LRRK2-PD, respectively). In summary, these results showed a decrease in the number of newly replicating mtDNA molecules together with an increase in their volume in both idiopathic and familial Parkinson's disease.

3.3. mtDNA transcription

Prompted by the results of lower mtDNA replication in both familial and idiopathic PD and on the basis of previous evidence suggesting that mtDNA replication and transcription may be mutually exclusive processes [23,24], we next measured mtDNA transcription using Selfie-dPCR [26]. This method enables separate analysis of transcriptional activity of each one of the mtDNA strands. Hence, we measured the absolute number of H- and L- strand transcripts and expressed the results in two different forms: as transcripts/mtDNA copy and transcripts/diploid genome, to control for changes in mtDNA copy number and in cell number respectively (Fig. 3b-e). Furthermore, to control for the accuracy of quantification of H- and L- transcripts, we used two different primer combinations targeting two different regions of the same template (Fig. 3a). The mt64-ND1 primer combination targets a region near the beginning of the H-strand transcript and the end of the L-strand transcript (between bases 3441 and 3504), whereas the mt92-CYTB primer combination targets a region near the beginning of the L-strand transcript and at the end of H-strand transcript (between bases 15,427–15,518) (Fig. 3a).

Strand-specific analysis of mtDNA transcripts with the mt64-ND1 primer pair showed that the number of H-strand transcripts was on average approximately 230% higher than L-strand transcripts in all groups combined. H-strand = 0·46 ± 0·098, $n = 42$, and L-strand = 0·14 ± 0·07, $n = 42$, transcripts/mtDNA copy. H-strand = 574 ± 120, $n = 47$, and L-strand = 173 ± 95, $n = 43$, transcripts/diploid genome. Comparison of H- and L- strand mtDNA transcription amongst the different patient groups showed that the number of mt64-ND1 H-strand transcripts was significantly higher in NMC, iPD and LRRK2-PD patients when compared to the NMNC control subjects either in transcripts/mtDNA copy (Fig. 3b) or in transcripts/diploid genome (Fig. 3c). For H-strand transcripts/mtDNA copy: NMNC = 0·38 ± 0·11, $n = 10$, 4 lines; iPD = 0·52 ± 0·07, $n = 9$, 4 lines (effect size d = 1·5); NMC = 0·47 ± 0·08, $n = 14$, 5 lines (effect size d = 0·9); LRRK2-PD = 0·47 ± 0·08 $n = 9$, 4 lines (effect size d = 0·9). For H-strand transcripts/diploid genome: NMNC = 481 ± 122, $n = 11$, 4 lines; iPD = 605 ± 137, $n = 11$, 4 lines (effect size d = 1); NMC = 616 ± 104, $n = 15$, 5 lines (effect size d = 1·2); LRRK2-PD = 579 ± 67, $n = 10$, 4 lines (effect size d = 1). In contrast, there were no significant differences in the number of mt64-ND1 L-strand transcripts amongst the four groups. L-strand transcripts/mtDNA copy: NMNC = 0·14 ± 0·10, $n = 8$, 4 lines; iPD = 0·19 ± 0·08, $n = 11$, 4 lines; NMC = 0·12 ± 0·05, $n = 13$, 5 lines; LRRK2-PD = 0·12 ± 0·06, $n = 10$, 4 lines. L-strand transcripts/diploid genome: NMNC = 153 ± 120, $n = 8$, 4 lines; iPD = 224 ± 94, $n = 11$, 4 lines; NMC = 165 ± 76, $n = 13$, 5 lines; LRRK2-PD = 144 ± 86 $n = 11$, 4 lines (Fig. 3b & c). To test whether any of the individual fibroblast lines had an influence on the increase in mt64-ND1 H strand transcription observed in iPD, NMC, and LRRK2-PD groups, we outlined the average number of mt64-ND1 transcripts per diploid genome for each line (Supplementary Fig. 2).

The results of transcription analyses with the mt92-CYTB primer pair were equivalent to those observed with the mt64-ND1 primer pair, but with a quantitative difference in L-strand transcription. The average amount of L-strand transcript measured at the region targeted by mt92-CYTB (0·29 ± 0·14, $n = 46$, L-strand transcripts/mtDNA copy and 294 ± 128, $n = 45$, L-strand transcripts/diploid genome) was significantly higher than the obtained by mt64-ND1 (0·14 ± 0·07 L-strand transcripts/mtDNA copy, effect size d = 1·4 and 173 ± 95 L-strand transcripts/diploid genome, effect size d = 1·8). Moreover, the number of mt92-CYTB H-strand transcripts was on average between 35 and 45% higher than L-strand transcripts in all groups combined. (0·41 ± 0·20H-strand transcripts/mtDNA copy, $n = 47$, and 0·29 ± 0·14 L-strand transcripts/mtDNA copy $n = 46$, effect size d = 0·7; 396 ± 180H-strand transcripts/diploid genome, $n = 49$ and 294 ± 128 L-strand transcripts/diploid genome, $n = 45$, effect size d = 0·7).

Likewise to the results observed with mt64-ND1, comparison of mt92-CYTB strand-specific transcription amongst the different patient groups showed that the number of H-strand transcripts was significantly higher in NMC, iPD and LRRK2-PD patients when compared to the NMNC control group when measured in both, transcripts/mt92-CYTB copy (Fig. 3d) or tran-

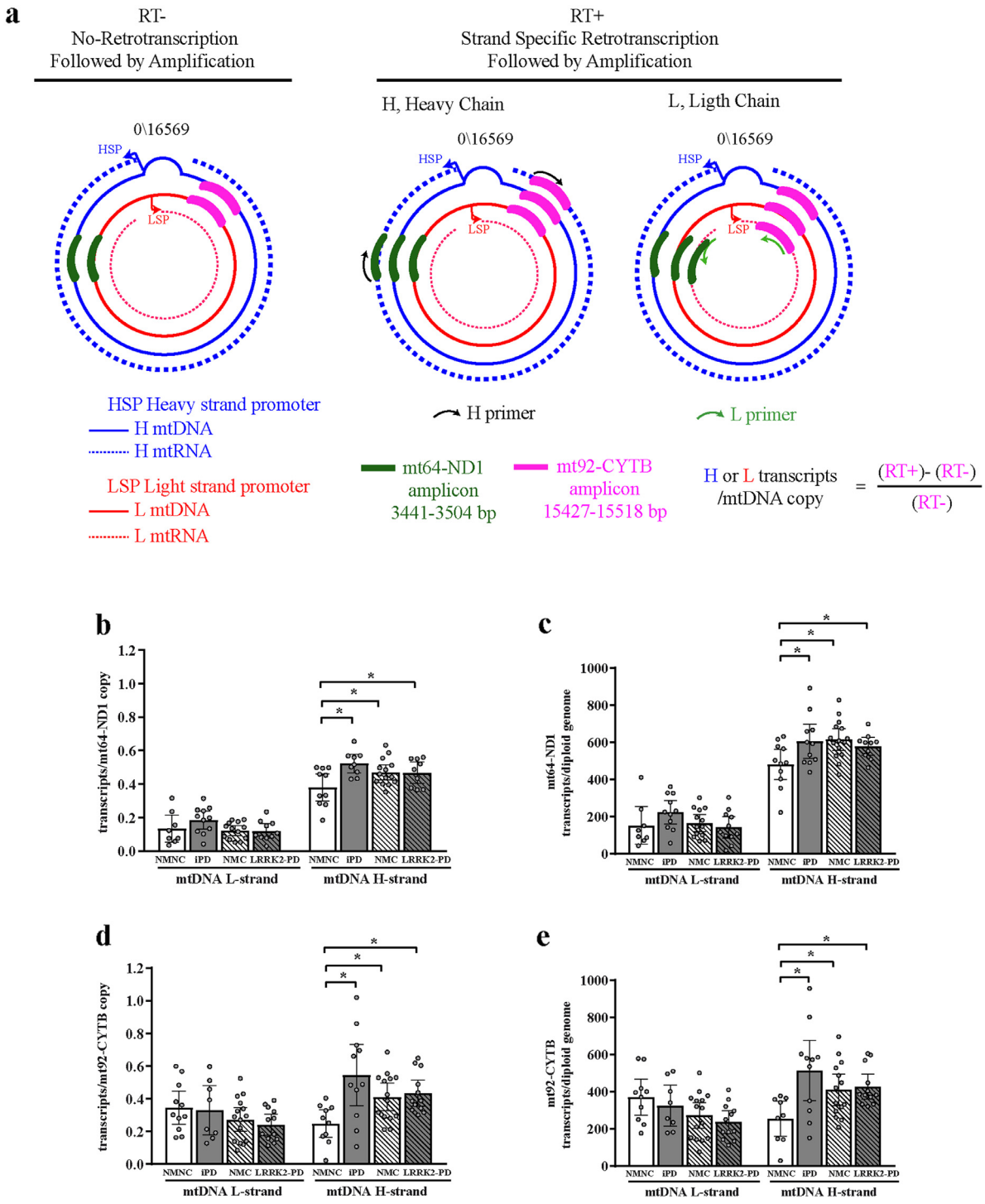

Fig. 3. Enhanced H strand mtDNA transcription in iPD and LRRK2-PD. a) Schematic diagram of strand specific analysis of mtDNA transcription using the Selfie-dPCR method, which allows for separate measurement of H- and L- strand transcripts (dotted lines) in relation to the mtDNA that encodes them (solid lines). The method includes four steps: 1) sample and strand-specific primer pre-annealing in duplicate (H primer = black arrow, L primer = green arrow), 2) reverse transcription without enzyme in one duplicate (RT-) and with enzyme (RT+) in the other duplicate, 3) digital PCR and 4) nucleic acid quantification. Two different primer combinations targeting two opposed regions of the same template (mt64-ND1 = thick green lines and mt92-CYTB = thick red lines) are used to test accuracy of H- and L- transcript quantification. The number of mtRNA transcripts per mtDNA copy are calculated by subtracting the amount of amplicons measured in RT- from RT+ and dividing by RT-. b & c) Quantification of mt64-ND1 strand specific transcription, expressed as transcripts/mtDNA copy in (b) and transcripts/diploid genome in (c), indicating that mt64-ND1 H-strand, but not L-strand, transcription was significantly higher in NMC, iPD and LRRK2-PD groups when compared to NMNC controls. (b: NMNC, $n = 10$, 4 lines; iPD $n = 9$, 4 lines, NMC $n = 14$, 5 lines, LRRK2-PD $n = 9$, 4 lines) (c: NMNC, $n = 11$, 4 lines, iPD $n = 11$, 4 lines, NMC $n = 15$, 5 lines, LRRK2-PD $n = 10$, 4 lines). d & e) Quantification of mt92-CYTB strand specific transcription, expressed as transcripts/mtDNA copy in (d) and transcripts/diploid genome in (e), confirming that mt92-CYTB H strand, but not L strand, transcription was significantly higher in NMC, iPD and LRRK2-PD groups when compared to NMNC controls. (d: NMNC, $n = 10$, 4 lines, iPD $n = 11$, 4 lines, NMC $n = 14$, 5 lines, LRRK2-PD $n = 12$, 4 lines) (e: NMNC, $n = 9$, 4 lines, iPD $n = 11$, 4 lines, NMC $n = 14$, 5 lines, LRRK2-PD $n = 12$, 4 lines). All data are mean and 95% CI. *, significantly different from the respective control group, $p < 0{\cdot}05$ (ANOVA with Fisher's LSD test). n denotes number of independent experiments. (For interpretation of the references to colour in this figure legend, the reader is referred to the web version of this article.)

scripts/diploid genome (Fig. 3e). For H-strand transcripts/mtDNA copy: NMNC = 0·25 ± 0·12, n = 10, 4 lines; iPD = 0·55 ± 0·28, n = 11, 4 lines (effect size d = 1·4); NMC = 0·41 ± 0·15, n = 14, 5 lines (effect size d = 1·2); LRRK2-PD = 0·44 ± 0·13 n = 12, 4 lines (effect size d = 1·5). For H-strand transcripts/diploid genome: NMNC = 255 ± 123, n = 9, 4 lines; iPD = 515 ± 242, n = 11, 4 lines (effect size d = 1·4); NMC = 410 ± 148, n = 14, 5 lines (effect size d = 1·1); LRRK2-PD = 428 ± 104, n = 12, 4 lines (effect size d = 1·5). In contrast, there were no significant differences in the number of L-strand transcripts/mtDNA copy between the four groups either in transcripts/mt92-CYTB copy (Fig. 3d) or transcripts/diploid genome (Fig. 3e). For L-strand transcripts/mtDNA copy: NMNC = 0·35 ± 0·15, n = 11, 4 lines; iPD = 0·33 ± 0·18, n = 8, 4 lines; NMC = 0·27 ± 0·13, n = 15, 5 lines; LRRK2-PD = 0·24 ± 0·10 n = 12, 4 lines. For L-strand transcripts/diploid genome, NMNC = 371 ± 136, n = 10, 4 lines; iPD = 325 ± 133, n = 8, 4 lines; NMC = 272 ± 124, n = 15, 5 lines; LRRK2-PD = 238 ± 96 n = 12, 4 lines (Fig. 3d & e).

Altogether, these results indicated an enhancement of H-strand transcription in fibroblasts from both iPD and LRRK2-PD groups without significant differences in L-strand transcription.

3.4. Evaluation of mtDNA deletions

To determine whether the differences in 7SDNA and H-strand transcription observed in iPD and LRR2-PD groups might be due to mtDNA deletions, we assessed mtDNA deletion levels by the ratio between a primer pair (mt88-ND4) that targets the common mtDNA deletion region and mt64-ND1. We compared this ratio with that of mt92-CYTB over mt64-ND1, the primer pairs used to measure mtDNA transcription, both targeting regions outside the mtDNA common deletion region. We found no significant amount of deletions in the region targeted by mt92-CYTB. In contrast, we found a significant amount of deletions (10% on average) in the region targeted by mt88-ND4 in all groups (Supplementary Fig. 3). These results indicate that mt92-CYTB targets an mtDNA sequence located outside of the common mtDNA deletion targeted by mt88-ND4. Moreover, these results suggest that the increase in 7SDNA and H-strand mtDNA transcription observed in iPD, NMC, and LRRK2-PD groups are unaffected by mtDNA deletions.

3.5. Cell free mtDNA release

We next measured the number of copies of cf-mtDNA released by fibroblasts to the cell culture medium. Preliminary studies showed that control fibroblasts release a low amount of cf-mtDNA during a 4 h period in fresh culture media, approximately 0·4 mtDNA copies per cell. To minimize the sampling error associated with low amount measurements and to obtain a precise evaluation of cf-mtDNA copy number we used simultaneously two different primer pairs in the same dPCR reaction: mt82-CYTB and mt92-CYTB, which target two different regions of the CYTB mtDNA gene (Fig. 4a). Initial characterization studies in fibroblast samples showed that these two primer pairs provided equivalent measures of mtDNA copy number. Using this combination of primer pairs, we found that iPD fibroblasts released a significantly lower amount of cf-mtDNA than fibroblasts from NMNC controls. NMNC = 0·43 ± 0·27, n = 8, 4 lines; iPD =0·24 ± 0·05, n = 11, 4 lines, mt82-CYTB+mt92-CYTB copies/diploid genome (effect size d = 1). Similarly, LRRK2-PD fibroblasts released less cf-mtDNA than corresponding NMC controls. NMC = 0·35 ± 0·15, n = 14, 5 lines; LRRK2-PD =0·21 ± 0·10, n = 12, 4 lines, mt82-CYTB+mt92-CYTB copies/diploid genome (effect size d = 1·1) (Fig. 4b & c). These effects were not associated with changes in cell death or proliferation, because there were no significant differences in cell number between groups. To determine the influence of cell metabolism on cf-mtDNA release, we investigated the effect of nutrient starvation by serum deprivation. A 4 h incubation of fibroblasts with serum free media induced a significant decrease in mtDNA copy number per cell in all groups (Fig. 4d). Control, mt92-CYTB copies/diploid genome: NMNC = 1498 ± 156, n = 12, 4 lines; iPD = 1564 ± 230, n = 12, 4 lines; NMC = 1683 ± 331, n = 15, 5 lines; LRRK2-PD = 1651 ± 184 n = 12, 4 lines. Serum deprivation, mt92-CYTB copies/diploid genome: NMNC = 1298 ± 121, n = 12, 4 lines (effect size d = 1·4, vs Control NMNC); iPD = 1290 ± 144, n = 12, 4 lines (effect size d = 1·4, vs Control iPD); NMC = 1430 ± 254, n = 15, 5 lines (effect size d = 0·9, vs Control NMC); LRRK2-PD = 1495 ± 174, n = 11, 4 lines (effect size d = 0·9). Likewise, serum deprivation produced a marked decrease of cf-mtDNA release to almost undetectable levels with no significant differences between groups (Fig. 4c).

In sum, these results showed that low cf-mtDNA release to the culture medium occurs both in iPD and LRRK2-PD fibroblasts and suggest that cf-mtDNA release does not result from cell lysis but that it is rather an active physiological process that may be regulated by metabolic stress.

4. Discussion

Here we report that primary fibroblasts obtained from patients with different subtypes of PD share a similar dysfunction of the mtDNA replication and transcription machinery. The study of mtDNA replication and transcription in live cells has been limited by the difficulty of accurately measuring the number of mitochondrial genome copies. To overcome this limitation, we developed a method called Selfie-dPCR that allows absolute quantification of the number of mitochondrial RNA transcripts relative to their own transcription chain in the mtDNA genome [26]. In addition, we implemented a multiplex digital PCR assay for absolute quantification of 7S DNA. Using these methods, we found that fibroblasts from patients with either idiopathic or LRRK2 PD showed a higher proportion of mtDNA molecules containing 7S DNA. The accumulation of 7S DNA in PD fibroblasts was associated with a decrease in mtDNA replication, with an increase in heavy strand mtDNA transcription and with a decrease in mtDNA release. These findings provide evidence that 7S DNA is part of a switch that toggles between mtDNA replication and transcription and suggest that alteration of this regulator is a fundamental pathophysiological mechanism that underlies both familial and idiopathic PD.

Absolute quantification of DNA strands within the mtDNA control region revealed that the proportion of mtDNA molecules containing 7S DNA in control fibroblasts was between 27 and 31%. This value, obtained with a novel method that does not require nucleic acid extraction, is within the range of previous data obtained with other methods in human tissues and cultured cells [33,34]. In addition, fibroblasts from patients with different forms of PD exhibited a 30% increase in the number of mtDNA molecules with 7S DNA, indicating that altered synthesis or degradation of 7S DNA is a molecular dysfunction that occurs in both idiopathic and familial PD fibroblasts.

The presence of 7S DNA in the mtDNA molecule may serve different functions, including initiation of H-strand replication and facilitation of mtDNA transcription (reviewed in [34]). To determine whether 7S DNA accumulation was associated with changes in mtDNA replication, we monitored EdU incorporation into mtDNA after direct labelling with click chemistry with a fluorescent Alexa Fluor dye. Fluorescence image analysis, combined with quantification of mtDNA copy number with dPCR, showed that the proportion of mtDNA molecules that incorporated EdU during a four-hour pulse in control fibroblasts was on average 5·7% (Fig. 2c), a value that is in close agreement with previous studies in mouse L cells [35]. However, the proportion of replicating mtDNA molecules was reduced significantly by 30% in fibroblasts from both idio-

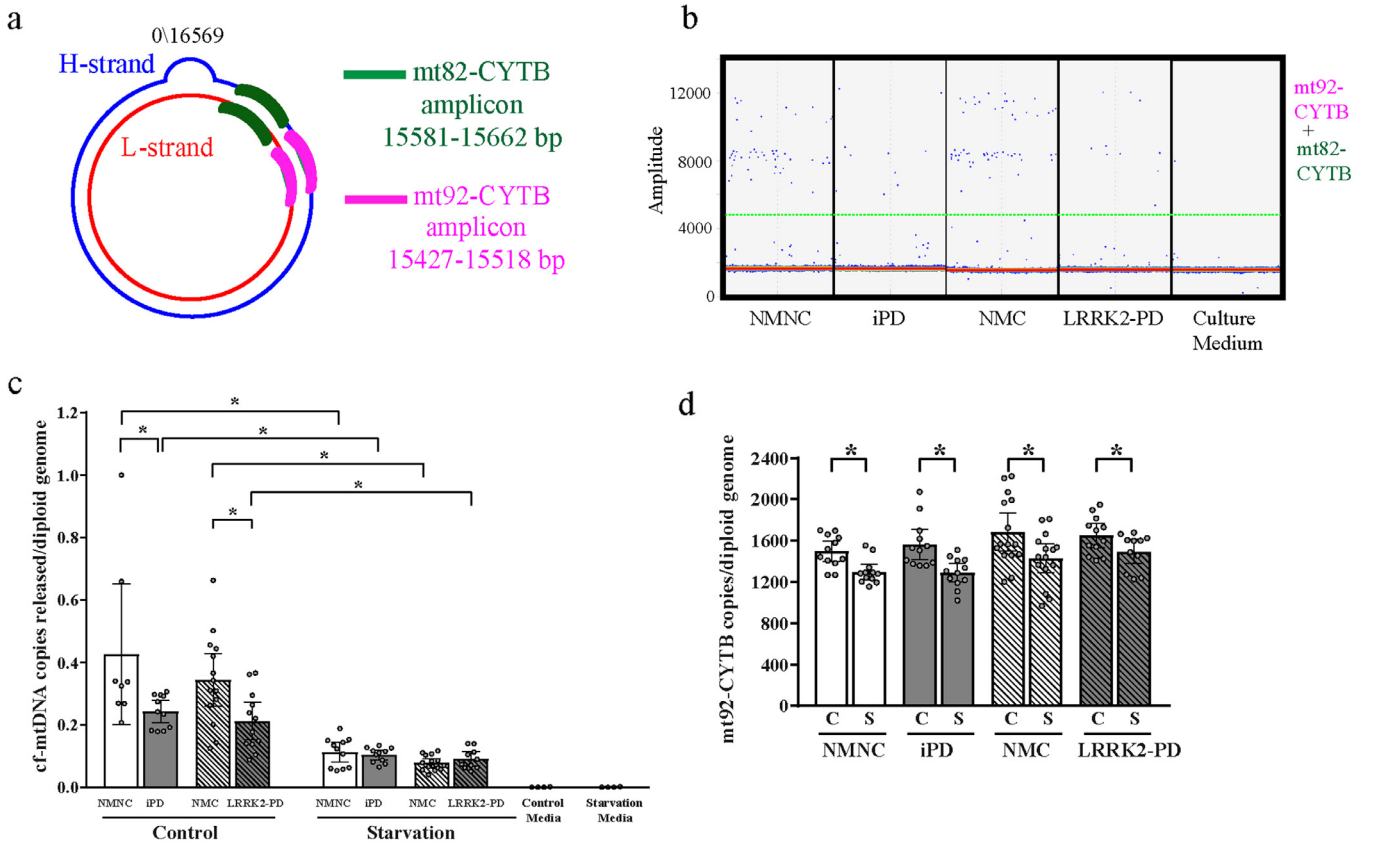

Fig. 4. Low release of cf-mtDNA in iPD and LRRK2-PD. Release of cf-mtDNA was measured in the culture medium after 4 h incubation. a) Schematic diagram of mtDNA regions amplified with two different primer pairs in the same dPCR reaction: mt82-CYTB and mt92-CYTB. The mt82-CYTB primer pair (thick green lines) and the mt92-CYTB primer pair (thick pink lines) were used in a multiplex dPCR assay to obtain an accurate evaluation of cf-mtDNA copy number. b) Representative 1-D droplet scatter plot of mt82-CYTB and mt92-CYTB amplicons after dPCR. Blue dots above an amplitude of 5000 indicate droplets positive for mt82-CYTB, mt92-CYTB or both of them. c) Graph showing that fibroblasts from PD patients released significantly less cf-mtDNA than their respective controls (NMNC $n = 8$, iPD $n = 11$, NMC, $n = 14$, LRRK2-PD $n = 12$). Nutrient starvation by serum deprivation decreased further cf-mtDNA release to almost undetectable levels in all groups (NMNC $n = 11$, iPD $n = 11$, NMC $n = 14$, LRRK2-PD $n = 10$). d) Graph showing that whereas groups do not differ in mtDNA copy number, 4 h of serum deprivation reduces mtDNA copy number in all groups. (NMNC $n = 12$, iPD $n = 12$, NMC $n = 15$, LRRK2-PD $n = 12$). The number of fibroblast lines in each group were: NMNC, 4 lines, iPD, 4 lines, NMC, 5 lines, LRRK2-PD, 4 lines. *, significantly different from the respective control group, $p < 0{\cdot}05$ (ANOVA with Fisher's LSD test). n denotes number of independent experiments. (For interpretation of the references to colour in this figure legend, the reader is referred to the web version of this article.)

pathic and LRRK2-related PD patients (Fig. 2b). These results indicate that in human fibroblasts, only a fraction of mtDNA molecules undergoes replication under normal physiological cellular conditions and that this fraction is downregulated in fibroblasts from PD patients. The mechanism involved in the regulation and selection of only a fraction of mtDNA molecules for replication is currently unknown, but our results show that dysregulation of this mechanism underlies different forms of PD. The finding that low mtDNA replication occurs in PD fibroblasts that accumulate 7S DNA provides support to the hypothesis that 7S DNA molecules, in addition to mtDNA replication, serve another function that is incompatible with mtDNA replication [23].

The average volume of mtDNA puncta labelled with EdU was significantly greater in fibroblasts from both iPD and LRRK2-PD patients. This effect was due to a decrease in the frequency of small and an increase in the frequency of large EdU puncta. One limitation of the morphological analyses in our studies is that the diffraction limit of images obtained with confocal microscopy does not enable an accurate measurement of EdU puncta size. However, the relative increase in the volume of EdU puncta observed in PD fibroblasts is consistent with the higher number of mtDNA molecules containing 7S DNA found in these cells. The presence of 7S DNA unwinds the mtDNA double strand by displacing the H-strand, creating a D-loop and a relaxed conformation of the mtDNA molecule [20]. Therefore, a higher number of relaxed open forms of mtDNA molecules containing 7S DNA could explain the increase in the average volume of EdU puncta in fibroblasts obtained from PD patients. An alternative explanation could be that large EdU puncta represent mtDNA aggregates produced by juxtaposition of newly replicated mtDNA molecules that cannot be resolved in confocal microscopy images [36]. However, the observation that mtDNA replication is lower in PD fibroblasts that have large EdU puncta argues against this possibility. Super-resolution microscopy studies have identified different forms and sizes of mtDNA nucleoids, which were hypothesized to depend on whether mtDNA was involved in active replication or transcription [37,38]. The interpretation that the large volume forms of EdU puncta found in our studies represent mtDNA molecules containing 7S DNA is in line with this hypothesis.

It has long been proposed that a major function of the D-loop is to facilitate transcriptional activity [21]. Hence, we investigated whether 7S DNA accumulation in PD fibroblasts is associated with changes in mtDNA transcription. Global analysis of strand-specific mtDNA transcription, including all fibroblast groups and using two different primer combinations, which target opposed transcript regions, revealed that the average amount of H-strand transcripts was higher than that of L-strand transcripts, independently of the primer combination used to measure them. The disparity between the number of H- and L- transcripts found in the present studies confirms our previous report showing asymmetrical transcription

of mtDNA strands in different tissues [26]. This disparity between H- and L- strand transcription is also consistent with another study using directional deep sequencing and RNA-seq in samples from cell lines and tissues [39]. Furthermore, comparison between control and PD fibroblasts showed that the number of H-strand transcripts was higher in fibroblasts from both iPD and LRRK2-PD groups, whereas there were no significant differences in L-strand transcription. The number of H- and L- strand transcripts measured by Selfie-dPCR represents a snapshot of the steady state of mtDNA transcription at the time of cell lysis. Thus, an increase in transcript number could represent changes in mtDNA transcription, maturation, stability or degradation. However, the increase in the number of H-strand transcripts found in fibroblasts from PD patients was equivalent in two opposed regions of the polycistronic transcript, one close to the H-strand promoter and the other at the end of the H-strand, which indicates that the high number H-transcripts is due to enhanced transcription, rather than to changes in transcript maintenance or degradation. The increase in H-strand transcription found in fibroblasts from PD patients without a concomitant change in L-strand transcription is likely to result in imbalance of oxidative phosphorylation complex I assembly that may lead to mitochondrial uncoupling. This hypothesis is consistent with a previous study showing that fibroblasts from patients with the $LRRK2^{G2019S}$ mutation exhibit lower mitochondrial potential, increased oxygen consumption and lower ATP levels characteristic of mitochondrial uncoupling [40].

Differentiated cells maintain a tight control of their mtDNA copy number by adjusting the mtDNA synthesis/degradation turnover rate [41]. The observation that low mtDNA replication in PD fibroblasts did not lead to a decrease in mtDNA copy number suggests that these fibroblasts adjust the dynamics of mtDNA turnover to compensate for low mtDNA replication. In support of this interpretation, fibroblasts from PD patients released significantly less cf-mtDNA to the culture medium than controls. The cf-mtDNA released by fibroblasts to the culture medium was not the result of cell death because cf-mtDNA release was in the absence of nuclear DNA. Notably, nutrient starvation by serum deprivation, which induces mitochondrial degradation and alters mtDNA turnover [42], caused a significant decrease in mtDNA copy number and markedly inhibited cf-mtDNA release in all fibroblast groups, implying that cf-mtDNA release is an active physiological process linked to the maintenance of mtDNA copy number.

The mechanisms involved in the release of cf-mtDNA to the extracellular space are still not well known. A recent study has shown that exhaustive exercise in Parkin or Pink knockout mice with impaired mitophagy increases mtDNA release [43], supporting the interpretation that mtDNA release is a by-product of defective mitophagy. This interpretation is consistent with our present findings showing that serum deprivation, which activates mitophagy, inhibits spontaneous cf-mtDNA release. Moreover, our results showing that the decrease in spontaneous mtDNA release in fibroblasts from iPD and LRRK2-PD patients is not additive to the one evoked by serum deprivation suggest that alteration of a quality control mechanism other than mitophagy mediates spontaneous cf-mtDNA release and that this quality control mechanism is particularly affected in PD.

The finding that mtDNA dynamics, including replication, transcription and release, is deregulated in non-neuronal cells, such as fibroblasts, obtained from patients with PD is consistent with previous reports showing that mitochondrial dysfunction is systemic in PD [7,8,44,45]. Moreover, the low mtDNA replication we observed in both iPD and LRRK2-PD fibroblasts (Fig. 2b & c) is in accordance with previous studies that have shown mtDNA depletion in single neurons from postmortem iPD brains [46,47], in substantia nigra pars compacta tissue from postmortem PD brains [14], and in peripheral blood from PD patients [14,48]. However, in contrast with some of the previous studies in postmortem tissue, our PD fibroblasts in culture, despite having low mtDNA replication, did not show mtDNA copy number depletion measured by two different primer combinations (mt64-ND1 and mt92-CYTB, Fig. 1e). Interestingly, low mtDNA replication in PD fibroblasts was associated with low spontaneous mtDNA release (Fig. 4c). This suggests a regulatory mechanism in live cells that preserves mtDNA copy number by reducing mtDNA release in response to low mtDNA replication. This mechanism and the ability to maintain mtDNA copy number may depend on the cell type and its metabolic state. For example, in contrast to the mtDNA depletion reported by different laboratories in neurons from substantia nigra pars compacta, mtDNA copy number is increased in surviving single pedunculopontine nucleus cholinergic neurons from post-mortem brains with PD [49].

Recent findings suggest that mtDNA major arc deletions are involved in LRRK2-PD penetrance [50]. However, a previous study did not detect significant differences in the number of mtDNA deletions in LRRK2-PD patients [51]. In the present study, mtDNA replication and transcription were assessed with two different primer pairs, mt92-CYTB and mt64-ND1, which target two opposite regions of the mtDNA genome that are outside the majority (>90%) of the mtDNA deletions [27,28]. While the mt92-CYTB primer pair targets a sequence proximal to L strand promoter and distal to the H strand promoter, the mt64-ND1 primer pair targets a sequence distal from L strand promoter and proximal to H strand promoter. However, to check whether mtDNA deletions influenced our results, we compared mtDNA deletion levels obtained from two different primer pair ratios: mt92-CYTB/mt64-ND1 and mt88-ND4/mt64-ND1, the latter targeting the common mtDNA deletion region. No significant amount of mtDNA deletions were present in the region targeted by mt92-CYTB. In contrast, there was a significant amount of deletions in all groups (10% on average) in the region targeted by mt88-ND4 (Supplementary Fig. 3), even though the number of mtDNA deletions did not differ between groups. These results indicate that the increase in 7SDNA and H-strand mtDNA transcription observed in iPD, NMC and LRRK2-PD groups are unaffected by mtDNA deletions. Nonetheless, further studies with a higher number of subjects from other LRRK2-PD cohorts will be necessary to confirm the present results.

In contrast with the present results obtained in fibroblasts, in a previous study, we found that the content of cf-mtDNA was increased in the cerebrospinal fluid of LRRK2-PD patients compared to unaffected LRRK2 mutation carriers [13]. Differences in cell type, metabolic state or quality control mechanisms might also explain the disparity between cf-mtDNA release in fibroblasts and the content of cf-mtDNA in cerebrospinal fluid. Indeed, the gene expression profile and the secretory vesicle pathways in fibroblasts are different in neurons (reviewed in [52]), highlighting the limitations of fibroblasts as a model to identify mechanisms of mtDNA release to the cerebrospinal fluid. Additionally, neurons are highly dependent on mitochondrial energy and, therefore, more susceptible than fibroblasts to damage caused by mitochondrial dysfunction. Accordingly, one limitation that applies to the studies reported here is that our findings may be restricted only to fibroblast cell lines. Recent advances in induced pluripotent stem cell and genome editing technologies will provide the opportunity to perform further studies to confirm whether the alteration in mtDNA dynamics found in fibroblasts from patients with PD also occurs in live neurons. In addition, one caveat from our study is that the genetic background of our patient cohort might have influenced our findings and more studies in other laboratories with distinct cohorts of PD patients are necessary. Nonetheless, our results suggest that the measurement of 7SDNA and its relationship with mtDNA replication and mtDNA transcription in fibroblasts may be an effective approach to investigate the biochemical pathways involved in

the dysregulation of mtDNA dynamics underlying PD and to identify new pharmacological targets.

Overall, the present results support the hypothesis that alteration of mtDNA dynamics is a key mechanism in the pathophysiology of PD. In summary, these results indicate that accumulation of 7S DNA is a molecular mechanism of mtDNA dysfunction shared by iPD and LRRK2-PD, and support the hypothesis that the genetic switch that alternates between mtDNA replication and transcription by regulating the levels of 7S DNA [23,24] plays a key role in both familial and idiopathic PD.

Funding sources

This work was supported by grants to Ramon Trullas and Petar Podlesniy from the Ministerio de Ciencia, Innovación y Universidades of Spain (Grant: SAF2017-89791-R) and from the Instituto Carlos III, Centro de Investigación Biomédica en Red Enfermedades Neurodegenerativas, CIBERNED (Grant: PI2016/06-3). The funders had no role in study design, data collection, data analysis, interpretation, or writing of the report.

Author contributions

Petar Podlesniy and Ramon Trullas contributed to all aspects of the study, including design, planning the experiments, analysing results and writing the manuscript. Núria Serra and Margalida Puigròs performed fibroblast cultures, dPCR analyses and analysed results. Rubén Fernández-Santiago, Mario Ezquerra and Eduardo Tolosa provided fibroblast samples and reviewed the manuscript.

Declaration of Competing Interest

PP, MP, NS, RFS, ME and RT have nothing to disclose.

ET received honoraria for consultancy from Novartis, TEVA, Bial, pAccorda, Boehringer Ingelheim, UCB, Solvay, Lundbeck, and BIOGEN. Grants from Spanish Network for Research on Neurodegenerative Disorders (CIBERNED)-Instituto Carlos III (ISCIII), and The Michael J. Fox Foundation for Parkinson's Research(MJFF), outside the submitted work.

Acknowledgements

We thank Dr. Inna Inashkina from the Medical Genetics and Mitochondrial Research group, Latvian Biomedical Research and Study Center, for help in studies with the mtDNA depleted cell line.

Appendix A. Supplementary data

Supplementary data to this article can be found online at https://doi.org/10.1016/j.ebiom.2019.09.015.

References

[1] Deng H, Wang P, Jankovic J. The genetics of Parkinson disease. Ageing Res Rev 2018;42:72–85.
[2] Paisan-Ruiz C, Lewis PA, Singleton AB. LRRK2: cause, risk, and mechanism. J Park Dis 2013;3(2):85–103.
[3] Zimprich A, Biskup S, Leitner P, Lichtner P, Farrer M, Lincoln S, et al. Mutations in LRRK2 cause autosomal-dominant parkinsonism with pleomorphic pathology. Neuron 2004;44(4):601–7.
[4] Healy DG, Falchi M, O'Sullivan SS, Bonifati V, Durr A, Bressman S, et al. Phenotype, genotype, and worldwide genetic penetrance of LRRK2-associated Parkinson's disease: a case-control study. Lancet Neurol 2008;7(7):583–90.
[5] Marder K, Wang Y, Alcalay RN, Mejia-Santana H, Tang MX, Lee A, et al. Age-specific penetrance of LRRK2 G2019S in the Michael J. Fox Ashkenazi Jewish LRRK2 Consortium. Neurology 2015;85(1):89–95.
[6] Mortiboys H, Thomas KJ, Koopman WJ, Klaffke S, Abou-Sleiman P, Olpin S, et al. Mitochondrial function and morphology are impaired in parkin-mutant fibroblasts. Ann Neurol 2008;64(5):555–65.
[7] Mortiboys H, Johansen KK, Aasly JO, Bandmann O. Mitochondrial impairment in patients with Parkinson disease with the G2019S mutation in LRRK2. Neurology 2010;75(22):2017–20.
[8] Hsieh CH, Shaltouki A, Gonzalez AE, Bettencourt da Cruz A, Burbulla LF, St Lawrence E, et al. Functional impairment in Miro degradation and mitophagy is a shared feature in familial and sporadic Parkinson's disease. Cell Stem Cell 2016;19(6):709–24.
[9] Kang E, Wang X, Tippner-Hedges R, Ma H, Folmes CD, Gutierrez NM, et al. Age-related accumulation of somatic mitochondrial DNA mutations in adult-derived human iPSCs. Cell Stem Cell 2016;18(5):625–36.
[10] Giannoccaro MP, La Morgia C, Rizzo G, Carelli V. Mitochondrial DNA and primary mitochondrial dysfunction in Parkinson's disease. Mov Disord 2017;32(3):346–63.
[11] Bose A, Beal MF. Mitochondrial dysfunction in Parkinson's disease. J Neurochem 2016;139(Suppl. 1):216–31.
[12] Ryan BJ, Hoek S, Fon EA, Wade-Martins R. Mitochondrial dysfunction and mitophagy in Parkinson's: from familial to sporadic disease. Trends Biochem Sci 2015;40(4):200–10.
[13] Podlesniy P, Vilas D, Taylor P, Shaw LM, Tolosa E, Trullas R. Mitochondrial DNA in CSF distinguishes LRRK2 from idiopathic Parkinson's disease. Neurobiol Dis 2016;94:10–17.
[14] Pyle A, Anugrha H, Kurzawa-Akanbi M, Yarnall A, Burn D, Hudson G. Reduced mitochondrial DNA copy number is a biomarker of Parkinson's disease. Neurobiol Aging 2016;38(216):e7–e10.
[15] Pyle A, Brennan R, Kurzawa-Akanbi M, Yarnall A, Thouin A, Mollenhauer B, et al. Reduced cerebrospinal fluid mitochondrial DNA is a biomarker for early-stage Parkinson's disease. Ann Neurol 2015;78(6):1000–4.
[16] Gustafsson CM, Falkenberg M, Larsson NG. Maintenance and expression of mammalian mitochondrial DNA. Annu Rev Biochem 2016;85:133–60.
[17] Falkenberg M. Mitochondrial DNA replication in mammalian cells: overview of the pathway. Essays Biochem 2018;62(3):287–96.
[18] Arnberg A, van Bruggen EF, Borst P. The presence of DNA molecules with a displacement loop in standard mitochondrial DNA preparations. Biochim Biophys Acta 1971;246(2):353–7.
[19] Kasamatsu H, Robberson DL, Vinograd J. A novel closed-circular mitochondrial DNA with properties of a replicating intermediate. Proc Natl Acad Sci U S A 1971;68(9):2252–7.
[20] Bogenhagen D, Clayton DA. Mechanism of mitochondrial DNA replication in mouse L-cells: kinetics of synthesis and turnover of the initiation sequence. J Mol Biol 1978;119(1):49–68.
[21] Clayton DA. Replication of animal mitochondrial DNA. Cell 1982;28(4):693–705.
[22] Clayton DA. Replication and transcription of vertebrate mitochondrial DNA. Annu Rev Cell Biol 1991;7:453–78.
[23] Agaronyan K, Morozov YI, Anikin M, Temiakov D. Mitochondrial biology. Replication-transcription switch in human mitochondria. Science 2015;347(6221):548–51.
[24] Kuhl I, Miranda M, Posse V, Milenkovic D, Mourier A, Siira SJ, et al. POLRMT regulates the switch between replication primer formation and gene expression of mammalian mtDNA. Sci Adv 2016;2(8):e1600963.
[25] Goetz CG, Tilley BC, Shaftman SR, Stebbins GT, Fahn S, Martinez-Martin P, et al. Movement Disorder Society-sponsored revision of the Unified Parkinson's Disease Rating Scale (MDS-UPDRS): scale presentation and clinimetric testing results. Mov Disord 2008;23(15):2129–70.
[26] Podlesniy P, Trullas R. Absolute measurement of gene transcripts with Self-ie-digital PCR. Sci Rep 2017;7(1):8328.
[27] Damas J, Samuels DC, Carneiro J, Amorim A, Pereira F. Mitochondrial DNA rearrangements in health and disease—a comprehensive study. Hum Mutat 2014;35(1):1–14.
[28] Belmonte FR, Martin JL, Frescura K, Damas J, Pereira F, Tarnopolsky MA, et al. Digital PCR methods improve detection sensitivity and measurement precision of low abundance mtDNA deletions. Sci Rep 2016;6:25186.
[29] Podlesniy P, Trullas R. Biomarkers in cerebrospinal fluid: analysis of cell-free circulating mitochondrial DNA by digital PCR. Methods Mol Biol 2018;1768:111–26.
[30] Schindelin J, Arganda-Carreras I, Frise E, Kaynig V, Longair M, Pietzsch T, et al. Fiji: an open-source platform for biological-image analysis. Nat Methods 2012;9(7):676–82.
[31] Bolte S, Cordelieres FP. A guided tour into subcellular colocalization analysis in light microscopy. J Microsc 2006;224(Pt 3):213–32.
[32] Salic A, Mitchison TJ. A chemical method for fast and sensitive detection of DNA synthesis in vivo. Proc Natl Acad Sci U S A 2008;105(7):2415–20.
[33] Kornblum C, Nicholls TJ, Haack TB, Scholer S, Peeva V, Danhauser K, et al. Loss-of-function mutations in MGME1 impair mtDNA replication and cause multisystemic mitochondrial disease. Nat Genet 2013;45(2):214–19.
[34] Nicholls TJ, Minczuk M. In D-loop: 40 years of mitochondrial 7S DNA. Exp Gerontol 2014;56:175–81.
[35] Bogenhagen D, Clayton DA. Mouse L cell mitochondrial DNA molecules are selected randomly for replication throughout the cell cycle. Cell 1977;11(4):719–27.
[36] Kukat C, Wurm CA, Spahr H, Falkenberg M, Larsson NG, Jakobs S. Super-resolution microscopy reveals that mammalian mitochondrial nucleoids have a uniform size and frequently contain a single copy of mtDNA. Proc Natl Acad Sci U S A 2011;108(33):13534–9.
[37] Brown TA, Tkachuk AN, Shtengel G, Kopek BG, Bogenhagen DF, Hess HF, et al. Superresolution fluorescence imaging of mitochondrial nucleoids re-

veals their spatial range, limits, and membrane interaction. Mol Cell Biol 2011;31(24):4994–5010.
[38] Kukat C, Davies KM, Wurm CA, Spahr H, Bonekamp NA, Kuhl I, et al. Cross-strand binding of TFAM to a single mtDNA molecule forms the mitochondrial nucleoid. Proc Natl Acad Sci U S A 2015;112(36):11288–93.
[39] Mercer TR, Neph S, Dinger ME, Crawford J, Smith MA, Shearwood AM, et al. The human mitochondrial transcriptome. Cell 2011;146(4):645–58.
[40] Papkovskaia TD, Chau KY, Inesta-Vaquera F, Papkovsky DB, Healy DG, Nishio K, et al. G2019S leucine-rich repeat kinase 2 causes uncoupling protein-mediated mitochondrial depolarization. Hum Mol Genet 2012;21(19):4201–13.
[41] Clay Montier LL, Deng JJ, Bai Y. Number matters: control of mammalian mitochondrial DNA copy number. J Genet Genomics 2009;36(3):125–31.
[42] Hirota Y, Yamashita S, Kurihara Y, Jin X, Aihara M, Saigusa T, et al. Mitophagy is primarily due to alternative autophagy and requires the MAPK1 and MAPK14 signaling pathways. Autophagy 2015;11(2):332–43.
[43] Sliter DA, Martinez J, Hao L, Chen X, Sun N, Fischer TD, et al. Parkin and PINK1 mitigate STING-induced inflammation. Nature 2018;561(7722):258–62.
[44] Yakhine-Diop SMS, Niso-Santano M, Rodriguez-Arribas M, Gomez-Sanchez R, Martinez-Chacon G, Uribe-Carretero E, et al. Impaired mitophagy and protein acetylation levels in fibroblasts from Parkinson's disease patients. Mol Neurobiol 56 (4) 2018:2466–81.
[45] Mortiboys H, Aasly J, Bandmann O. Ursocholanic acid rescues mitochondrial function in common forms of familial Parkinson's disease. Brain 2013;136(Pt 10):3038–50.
[46] Grunewald A, Rygiel KA, Hepplewhite PD, Morris CM, Picard M, Turnbull DM. Mitochondrial DNA depletion in respiratory chain-deficient Parkinson disease neurons. Ann Neurol 2016;79(3):366–78.
[47] Dolle C, Flones I, Nido GS, Miletic H, Osuagwu N, Kristoffersen S, et al. Defective mitochondrial DNA homeostasis in the substantia nigra in Parkinson disease. Nat Commun 2016;7:13548.
[48] Gui YX, Xu ZP, Lv W, Zhao JJ, Hu XY. Evidence for polymerase gamma, POLG1 variation in reduced mitochondrial DNA copy number in Parkinson's disease. Parkinsonism Relat Disord 2015;21(3):282–6.
[49] Bury AG, Pyle A, Elson JL, Greaves L, Morris CM, Hudson G, et al. Mitochondrial DNA changes in pedunculopontine cholinergic neurons in Parkinson disease. Ann Neurol 2017;82(6):1016–21.
[50] Ouzren N, Delcambre S, Ghelfi J, Seibler P, Farrer MJ, Konig IR, et al. Mitochondrial DNA deletions discriminate affected from unaffected LRRK2 mutation carriers. Ann Neurol 2019;86(2):324–6.
[51] Howlett EH, Jensen N, Belmonte F, Zafar F, Hu X, Kluss J, et al. LRRK2 G2019S-induced mitochondrial DNA damage is LRRK2 kinase dependent and inhibition restores mtDNA integrity in Parkinson's disease. Hum Mol Genet 2017;26(22):4340–51.
[52] Auburger G, Klinkenberg M, Drost J, Marcus K, Morales-Gordo B, Kunz WS, et al. Primary skin fibroblasts as a model of Parkinson's disease. Mol Neurobiol 2012;46(1):20–7.